The spatiotemporal variation and control mechanism of surface pCO2 in winter in Jiaozhou Bay, China

The spatiotemporal variation and control mechanism of surface pCO_2 in winter in Jiaozhou Bay, China

Yunxiao Li[a], Hong Yang[b], Longjun Zhang[c*], Xufeng Yang[d], Han Zang[e], Wenhua Fan[a], Gailing Wang[a]

[a] Environment Science Laboratory, College of Resource and Environment, Shanxi Agricultural University, Taigu 030801, China

[b] Department of Geography and Environmental Science, University of Reading, Whiteknights, Reading RG6 6AB, UK

[c] Key Laboratory of Marine Environmental Science and Ecology, Ministry of Education, College of Environmental Science and Engineering, Ocean University of China, Qingdao 266100, China

[d] Second Institute of Oceanography, Ministry of Natural Resources, Hangzhou 310012, China

[e] College of Environmental Science and Engineering, Shanghai Jiao Tong University, Shanghai 200240, China

[*] Corresponding author at: College of Environmental Science and Engineering, Ocean University of China, Qingdao 266100, China.

E-mail address: longjunz@ouc.edu.cn (L Zhang).

Abstract

In many mid-latitude coastal waters during winter months, in addition to temperature, the large change in biogeochemical processes often influence and complicate the surface partial pressure of CO_2 (pCO_2). Based on the hydrological and carbonate parameters in seven cruises, this study analysed the evolution process and explored the control mechanism of the surface pCO_2 in Jiaozhou Bay, China, from December to March. The results showed that the pCO_2 ranged from 157 μatm to 647 μatm, and the bay represented a sink for atmospheric CO_2 (-3.8 mmol m^{-2} d^{-1}) in the whole winter. The non-temperature processes were the dominant factors affecting intra-winter pCO_2 variation. In December, the bay was dominated by aerobic respiration and acted as a CO_2 source (3.0 mmol m^{-2} d^{-1}). From early January to late February, however, the vigorous growth of cold algae caused strong primary production, and the bay presented as a CO_2 sink (from -6.4 mmol m^{-2} d^{-1} in early January to -15.5 mmol m^{-2} d^{-1} in late February). In March, primary production weakened and the effects of the $CaCO_3$ precipitation appeared, and the strength of the CO_2 sink was obviously weakened (-1.1 mmol m^{-2} d^{-1}). Meanwhile, the water temperature decreased gradually from December to late January and then increased until March, and it further expanded the variation range of pCO_2. Our results highlight the obvious source/sink change in mid-latitude seawater CO_2 in winter, while more field observations are still needed to further understand the complicated biogeochemical processes and its influence on seawater pCO_2.

Keywords: pCO_2; Aerobic respiration; Primary production; $CaCO_3$ precipitation; Controlling mechanism; Jiaozhou Bay

1. Introduction

The absorption intensity of CO_2 in coastal waters has received increasing attention (Borges, 2011; Cai et al., 2011; Gruber, 2015). The current estimate accounts for 10~20% of the CO_2 absorbed by the world's oceans (Chen et al., 2013; Laruelle et al., 2014; Wanninkhof et al., 2013). However, the rapid change in biogeochemical processes produces large uncertainties in the estimates. Therefore, a more comprehensive and in-depth understanding of the spatiotemporal pattern and mechanisms controlling coastal CO_2 system is extremely necessary.

In winter, a decrease in seawater temperature increases the solubility of CO_2, resulting in a decrease in the surface partial pressure of CO_2 (pCO_2). In most of the mid-latitude sea areas in the world, the temperature variation from summer to winter accounts for more than 50% of the change in pCO_2 (Takahashi et al., 2002). Many studied areas, such as the western area of the North Atlantic Ocean (Heike et al., 2004), the North Sea (Thomas et al., 2005), the US South Atlantic Bight (Jiang et al., 2013) and the North Yellow Sea (Xue et al., 2012), have shown that low temperature in winter often results in low pCO_2 levels, and some ocean areas even appear as sinks of atmospheric CO_2. However, affected by the coupled influence of low temperature, vertical mixing, runoff variation, nutrient supply and light intensity in winter, vigorous growth of phytoplankton often occurs in many mid-latitude coastal waters, such as the waters near Blanca (Argentina) in South America (Popovich et al., 2008), the Narragansett Bay and the Sargasso Sea in North America (Oviatt et al., 2002; Tin et al., 2016), the waters near the Loire estuary and the Adriatic Sea in Europe (Guillaud et al., 2008; Ljubimir et al., 2017), and the nearshore areas of the Bohai Sea and the Hokkaido in North-east Asia (Sakamoto et al., 2008; Zhao et al., 2004). In addition, a certain degree of aerobic respiration occurs in some areas, for example, the central area of the Baltic Sea and the North Yellow Sea (Wesslander et al., 2010; Xu et al., 2016). Therefore, in addition to the effects of temperature variation, the influence of non-temperature biogeochemical processes on the CO_2 source/sink change should not be neglected in mid-latitude coastal waters in winter.

The CO_2 sinks caused by primary production in winter have been reported in some mid-latitude coastal waters. In the Patagonia Sea in South America, Bianchi et al. (2009) conducted a cruise survey in winter. Their results showed that pCO_2 values had a significant negative correlation with Chlorophyll a (Chl *a*), and the region of 60~61.1°W with the highest Chl *a* value of >3.5 μg/L acted as a sink of atmospheric CO_2. In the nearshore areas of the Loire estuary, based on one cruise data in February, Bozec et al. (2012) found that the increase in river discharge promoted the vertical stratification of seawater and brought large amounts of nutrients. Consequently, the phytoplankton bloom consisting mainly of diatoms caused the seawater surface pCO_2 to be lower than the atmosphere by 42 μatm. Regarding the phenomenon of an increase in pCO_2 caused by aerobic respiration, Xu et al. (2016) found that vertical mixing carried the subsurface organic matter to the

surface layer and aerobic respiration made the northern Yellow Sea act as a CO_2 source in December (the average pCO_2 was 464 μatm). In spite of some field observation in different areas, more cruise surveys and analyses are still needed to more comprehensively reveal the detailed spatiotemporal pattern of pCO_2 and its control mechanisms throughout the winter months.

Jiaozhou Bay (JZB) (35°18'~36°18'N, 120°04'~120°23'E) is a typical mid-latitude semi-closed shallow water in northern China. The water area is 302.9 km^2 and the average water depth is 7 m. The climate is dominated by the East Asia Monsoon, with northerly wind in winter and southerly wind in summer (Li et al., 2006). The tidal current is a regular semi-diurnal tide that induces strong vertical mixing and good vertical homogeneity of the seawater temperature and salinity (Chen et al.,1999; Liu et al., 2004). The bay is an ideal area for characterizing the natural variation in pCO_2 and understanding their controlling processes, particularly in winter. First, as a typical mid-latitude water body, JZB has a strong seasonal change of physically properties. In particular, the average seawater surface temperature increases by ~ 10 °C from winter to spring (Li et al., 2007). Second, approximately 37% of the human population in the world lives within 100 km of the coastline (Cohen et al., 1997) and especially in the mid-latitude area, making this area subject to intense human impact (Bauer et al., 2013). JZB is a typical bay that is highly affected by urbanization. The eastern area of the bay is adjacent to the downtown of Qingdao City, with a population of 4.8 million, and the major estuaries (Licun River, Haibo River and Loushan River) have already become conduits for wastewater (Gao et al., 2008). Large amounts of nutrient and organic pollutant input have caused eutrophication and other problems in the JZB, with strong influence on carbon cycle in the area (Wang and Wang, 2011). The measurement of phytoplankton biomass, determined by using Chl *a*, in the past two decades indicated a clear bimodal pattern with peaks in summer and winter in the bay (Sun et al.,2011a; Wang et al., 2015; Wu et al., 2004). Same as many coasts in China, JZB is also an important shellfish-farming area with a breeding area of 107 km^2 (Yang et al., 2007; Zhang et al., 2005), suggesting the possible effect of calcification on pCO_2.

In the previous studies on controlling mechanisms of pCO_2 in the JZB during winter, Zhang et al. (2012) conducted one cruise in autumn and the other in winter. Their results indicated that the

bay experienced a process of intense organic degradation in autumn and strong primary production in winter, causing the bay from a CO_2 source to a sink during the period. Recently, Zang et al. (2018) found that the decrease in seawater temperature and enhancement of primary production together resulted in the bay acting as a CO_2 sink. However, pCO_2 changes throughout the winter and the mechanism for the variation are far from clearly understood. To fill the knowledge gap, this study researched the variation in seawater surface pCO_2 from December to March in the JZB and explored the factors determining the change of pCO_2. In particular, this study analysed the effect of the biogeochemical process induced by phytoplankton bloom on CO_2 source/sink patterns, with the consideration of water temperature variation (decrease first and increase later). The results can improve the understanding of the pCO_2 control mechanism in mid-latitude coastal waters where strong biological activities occur in winter.

2. Material and methods

2.1 Survey stations and sample processing

Seven cruises were conducted in the JZB during winter from 2008 to 2016. Survey time and number of stations are listed in Table 1. In each cruise, samples were collected from 24~33 stations (Figure 1). During the cruises, seawater samples were collected from the water surface at a depth of approximately 1.5 m because of the homogeneous vertical profiles in the JZB water column (Chen et al., 1999). Seawater surface temperature, salinity, oxygen saturation (DO%) and pCO_2 data were collected continuously, and discrete water samples were collected using 5 L Niskin bottles for later analysis of dissolved inorganic carbon (DIC), total alkalinity (TA), and Chl *a*.

Surface temperature and salinity were measured using a SBE 45 Micro TSG (Sea-Bird, Inc., Bellevue, WA, USA), with a nominal precision of 0.002 °C for temperature and 0.005 for salinity. The DO% was measured with a YSI-5000 oxygen analyser (YSI Corporation, Yellow Spring, OH, USA), which was calibrated using the Winkler titration method (nominal precision: 0.1%). The surface pCO_2 was measured with a non-dispersive infrared (NDIR) spectrometer (Li-Cor Model Li-7000, Lincoln, NE, USA) or a G2131-I Analyser (PICAROO, USA) using wavelength-scanned cavity ring-down spectroscopy (WS-CRDS), coupled to an equilibrator. The pCO_2 data in cruises before 2014 were measured using a Li-7000 NDIR spectrometer with a measurement uncertainty of

less than 1%, and those in 2014 and after were measured using a G2131-I Analyser with a nominal precision of < 50 ppbv over 5-min intervals. Before and after each cruise, the pCO_2 measurement instruments were calibrated against three CO_2 gas standards (202, 401 and 1010 ppm CO_2 in air) and one N_2 reference (National Research Center for Certified Reference Materials, Beijing, China).

To measure DIC and TA of water samples, filtration treatment was needed to avoid the influence of the particular matter. The DIC samples were directly collected from the Niskin bottles using a syringe and filtered through a 0.45 μm disposable syringe filter to avoid exchange with the air. TA samples were filtered through cellulose acetate membranes (0.45 μm) using a borosilicate glass filter. The DIC and TA samples were all poisoned with saturated mercury chloride (final concentration: *c.* 0.02% by volume) and preserved at 4 °C (Li et al., 2017). The DIC values were determined by acid extraction using a total organic analyser (TOC-VCPN, Shimadzu Corporation, Kyoto, Japan) (Liu et al., 2014) or a DIC analyser (AS-C2, Apollo SciTech, USA). The TA values were determined by Gran titration using a Total Alkalinity Titrator (AS-ALK2, Apollo SciTech, USA). Measurements of DIC and TA were both calibrated against Certified Reference Materials (CRMs) from Scripps Institution of Oceanography at a precision and accuracy level of 0.2%.

Samples for Chl *a* measurement were filtered through GF/F glass fibre membranes (0.7 μm; Whatman, Maidstone, UK) at pressures below 0.04 MPa. Saturated magnesium carbonate was added to the membranes after filtration, and the samples were preserved at -20 °C. Before analysis, the samples were extracted with 90% acetone, and the supernatant fluid was analysed using a fluorescence spectrophotometer (F4500, Hitachi Co, Tokyo, Japan).

2.2. Methodology

2.2.1. Aragonite saturation state

The aragonite saturation state (Ω_{arag}) at *in situ* temperatures (Ω_{arag}@situ) was calculated from the DIC, TA, *in situ* temperature, and *in situ* salinity values using the CO_2 program (Lewis and Wallace, 1998) and the CO_2 system coefficients of Mehrbach et al. (1973) as refitted by Dickson and Millero (1987). The Ksp* values for aragonite were taken from Mucci (1983), and the Ca^{2+} concentrations were assumed to be proportional to salinity, as presented in Millero (1979).

2.2.2. pCO_2 normalization

Considering that our pCO_2 data were collected over several years, this study normalized the surface water pCO_2 values of the cruises in December to the year 2015 and those of other cruises to the year 2016 by assuming that seawater surface pCO_2 increased at the same growth rate (1.5 μatm yr^{-1}) of the pCO_2 in the air according to Nakaoka et al. (2006).

2.2.3. The temperature effect on pCO_2

To assess the temperature effect on the distribution of pCO_2 in each cruise, this study normalized the observed *in situ* pCO_2 data to the average seawater temperature of the corresponding cruise using the equations proposed by Takahashi et al. (1993), and then temperature-normalized pCO_2 ($npCO_2$) was calculated:

$$npCO_2 = (pCO_2)_{obs} \times EXP[0.0423 \times (T_{nor} - T_{obs})] \quad (1)$$

where $(pCO_2)_{obs}$, T_{obs} and T_{nor} are the observed *in situ* surface pCO_2, *in situ* temperature and the temperature to which the *in situ* pCO_2 needs to be normalized, respectively. Then, the difference between $npCO_2$ and $(pCO_2)_{obs}$ was the temperature effect on pCO_2 distribution in the cruise.

Similarly, to assess the temperature effect on pCO_2 between the cruises, the average pCO_2 for each cruise was normalized to the average seawater temperature of all cruises. Then, the pCO_2 in each cruise under the average seawater temperature in winter ($NpCO_2$) was calculated:

$$NpCO_2 = (pCO_2)_{mean} \times EXP[0.0423 \times (T_{Mean} - T_{mean})] \quad (2)$$

where $(pCO_2)_{mean}$ and T_{mean} are the average surface pCO_2 and temperature in each cruise. T_{Mean} is the average seawater temperature of all cruises.

To assess the relative importance of temperature and non-temperature effect (including the effect of biological activities) on pCO_2 between the cruises, this study used equations developed by Takahashi et al. (2002):

$$T: pCO_2 \text{ at } T_{obs} = (pCO_2)_{Mean} \times EXP[0.0423 \times (T_{obs} - T_{Mean})] \quad (3)$$

$$B: pCO_2 \text{ at } T_{Mean} = (pCO_2)_{obs} \times EXP[0.0423 \times (T_{Mean} - T_{obs})] \quad (4)$$

$$\Delta(pCO_2)_{non\text{-}temp} = (pCO_2 \text{ at } T_{Mean})_{max} - (pCO_2 \text{ at } T_{Mean})_{min} \quad (5)$$

$$\Delta(pCO_2)_{temp} = (pCO_2 \text{ at } T_{obs})_{max} - (pCO_2 \text{ at } T_{obs})_{min} \quad (6)$$

where $(pCO_2)_{Mean}$ is the average pCO_2 of all cruises, and the subscripts "max" and "min" indicated the maximum and minimum values, respectively.

The relative importance of each effect can be expressed in terms of the ratio between the temperature effect (T) and non-temperature effect (B):

$$T / B = \Delta(pCO_2)_{temp} / \Delta(pCO_2)_{non\text{-}temp} \quad (7)$$

2.2.4. Statistical analyses

The correlations between environmental variables were analysed using SPSS 21 (IBM SPSS Statistics, IBM Corporation, Armonk, New York). All statistical analyses were at significance level of 0.05.

3. Results

3.1 Temperature and salinity

The seawater temperature in the JZB in winter is shown in Figure 2. The temperatures in the seven cruises surveyed were all below 10 °C, and the average temperature decreased from 7.1 °C in December to 1.5 °C in late January and then gradually increased to 8.6 °C in March. The time span of seven cruises (8 years) was relatively large. Compared with the multi-year diurnal average seawater temperature data in the JZB during winter, the temperature in the five cruises from December to late January was slightly lower and that in March. Even so, the overall variation trends of temperature in these cruises were consistent with the changes of daily seawater temperature, showing that these cruise data had a certain representativeness and can be used to analyse the pCO_2 variation between winter months in the JZB. The temperature increased from the upper end of the bay to the mouth of the bay in the five cruises from December to late January (Figure 3). The temperature gradient in each cruise in this period was relatively large, and the difference between the lowest and the highest temperature values all exceeded 4.0 °C. The temperature values in the two cruises during December were the highest (4.4~9.0 °C and 3.9~9.7 °C), while the temperature values in the cruise in late January were the lowest (-1.3~4.6 °C). In late February, due to the impact of land warming, no obvious temperature difference between the upper end of the bay and the mouth area existed. The temperature in this period was evenly distributed with a range of 3.8~4.7 °C. In

March, the temperature decreased from the upper end of the bay to the mouth, with a range of 7.7~9.9 °C.

The seawater surface salinity values in December and early January were relatively close and were basically between 29.0 and 30.9 (Figure 2). In the four cruises from mid-January to March, the salinity levels were higher with values of >30.3. In late January, the salinity values were the highest throughout the winter and ranged from 30.9 to 31.7. In late February and March, the salinity decreased slightly, and the ranges were 30.3~31.2 and 30.5~31.2, respectively. In terms of distribution in these seven cruises (Figure 3), the salinity increased from the northeastern area to the mouth, and the difference between the highest and lowest values in each cruise was less than 2.0. The salinity in the northeastern area was always the lowest, and the gradient variation was relatively large, indicating the influence of terrestrial input. The rivers entering the JZB have no natural runoff and the winter is the dry season. However, three wastewater treatment plants located near the northeastern area and the daily total amount of treated sewage is up to ~510000 tons, indicating that the direct treated sewage input was the main reason for the low salinity in this region.

3.2 pCO_2

The distribution of seawater surface pCO_2 in the JZB in winter is shown in Figure 4. According to the average air CO_2 data (408 μatm) from December 2015 to March 2016 from the flask measurements on the Tae-ahn Peninsula (126.131°E, 36.731°N) adjacent to the southern Yellow Sea, the bay in two cruises during December acted as a source of atmospheric CO_2 as a whole, and the pCO_2 ranges were 379~536 μatm and 382~647 μatm, respectively. The pCO_2 gradually decreased from the northeastern area to the mouth area. Obviously, the pCO_2 in the northeastern area was the largest (>450 μatm). In early January, the pCO_2 value was between 216 μatm and 520 μatm. The northeastern area also acted as a CO_2 source, but the western area was unsaturated with respect to atmospheric CO_2. In mid-January (282~375 μatm), late January (202~324 μatm) and late February (157~327 μatm), the CO_2 levels in the entire bay were all unsaturated and the pCO_2 decreased from the mouth to the northeastern area. The pCO_2 value in the northeastern area was even below 190 μatm in late February. In March, the bay acted as a weak CO_2 sink as a whole with the pCO_2 values of 357~415 μatm. The pCO_2 value was highest in the northern area and decreased gradually to the

mouth area, while the difference of pCO_2 between areas did not exceed 50 μatm. Overall, the pCO_2 values throughout the winter showed a process of gradual decrease from December to the end of February and then obvious increase in March (Figure 4h). The average pCO_2 value of all cruises was 352 μatm. Therefore, the bay acted as a sink of atmospheric CO_2 in winter as a whole.

3.3 DO% and Chl *a*

The distribution of seawater surface DO% in the JZB in winter is shown in Figure 5. The seawater surface DO in the JZB was unsaturated in both cruises in December (ranges: 79.8~98.1% and 79.5~101.5%) and increased from the northeastern area to the mouth area. In the northeastern area, which acted as the strongest CO_2 source, the unsaturated degree of DO was the highest and the DO% values were approximately 85%, showing the presence of aerobic respiration. In early January, DO remained unsaturated in the northeastern area which acted as a CO_2 source, but oversaturated (~105%) in the western area which acted as a CO_2 sink. In mid-January, late January and late February, when the entire JZB acted as a CO_2 sink, the DO% ranges were 101.0~117.5%, 109.4~120.2% and 102.0~147.0%, respectively. In these three cruises, DO was oversaturated and decreased from the northeastern area to the mouth area. Moreover, in the northeastern area, DO% values were highest and were above 110% (mid-January), 115% (late January) and 125% (late February), respectively, showing a strong primary production process. In March, the DO was slightly oversaturated with DO% values of 103.2~114.8%. The DO% distribution in the bay was relatively uniform, and the values in most areas were approximately 109.0%. Overall, the variation trend of DO% throughout the winter was opposite to pCO_2, a process of gradual increase from December to late February and then decrease in March (Figure 5h).

The distribution of seawater surface Chl *a* in the JZB in winter is shown in Figure 5. The Chl *a* concentration was low and below 0.60 μg/L in December when the DO was unsaturated. The ranges of Chl *a* in these two cruises were 0.03~0.61 μg/L and 0.12~0.55 μg/L, respectively. In early January, the Chl *a* concentrations in the western and mouth areas were above 0.60 μg/L. In mid-January, late January and late February, when the DO in the entire bay was oversaturated, the ranges of Chl *a* were 0.30~2.30 μg/L, 0.40~9.12 μg/L and 1.78~8.94 μg/L, respectively. The Chl *a* concentrations in the three cruises all decreased from the northeastern area to the mouth, and the

Chl *a* concentrations in the northeastern area were above 1.50 μg/L, 4.50 μg/L and 6.50 μg/L, respectively. In March, when the DO was slightly oversaturated, the Chl *a* concentration was lower with Chl *a* values of 0.04~0.40 μg/L. Overall, the variation of phytoplankton biomass represented by Chl *a* concentration throughout the winter was in good agreement with that of DO%, showing a process of gradual increase from December to the end of February and then obvious decrease in March (Figure 5h).

3.4 DIC and TA

The seawater surface DIC in the JZB in winter is shown in Figure 6. In December and early January, the DIC levels were relatively high and generally ranged between 2100 μmol/kg and 2300 μmol/kg. The DIC values were highest in the northeastern area and decreased gradually to the mouth, with the difference of approximately 150 μmol/kg. In these two periods, the difference in DIC distribution mainly occurred in the western area of the bay. In December, the DIC in the western area was approximately 40 μmol/kg higher than that in the mouth, but they were close in early January. In middle and late January, the DIC values (2142~2156 μmol/kg and 2130~2155 μmol/kg) were lower than those in December. The DIC also decreased from the northeastern area to the mouth area, but the difference between two areas was much smaller, just ~15 μmol/kg. In late February, the DIC values were the lowest throughout the winter, with a range of 2000~2140 μmol/kg. The DIC value increased gradually from the northeastern area to the mouth area and the difference was up to ~90 μmol/kg. In March, the DIC values (2085~2126 μmol/kg) also maintained a lower level but increased from the north area to the mouth area, with the difference of ~20 μmol/kg between two areas.

Seawater surface TA in the JZB during winter is shown in Figure 6. In December and early January, the TA values ranged generally between 2240 μmol/kg and 2400 μmol/kg. The spatial distribution of TA was similar to that of DIC. The TA values were also highest in the northeastern area and decreased gradually to the mouth. However, the decreasing gradient of TA was slightly smaller than that of DIC, and the TA difference between the northeastern and the mouth area was approximately 110 μmol/kg. In early January, TA values in the western area (where DIC values were close to those in the mouth area) were ~30 μmol/kg higher than those in the mouth area. In middle

and late January, the TA ranges were 2297~2336 μmol/kg and 2302 ~2360 μmol/kg, respectively. Compared to December, the TA values of these two cruises were slightly higher in most areas except for the northeastern area, and the TA difference between the northeastern area and the mouth area was only ~45 μmol/kg. In late February, the TA was between 2302 μmol/kg and 2364 μmol/kg, and the spatial distribution was opposite to that of DIC. The TA value was highest in the northeastern area with low DIC and increased gradually to the mouth area. In March, the TA value ranged from 2290 μmol/kg to 2347 μmol/kg. Spatial distribution of TA was similar to that of DIC, and the TA values increased from the northern area to the mouth area. However, the change gradient of TA was larger than that of DIC, and the TA values in the northern area were ~40 μmol/kg lower than those in the mouth.

4. Discussion

4.1 The temperature effect on variation in surface pCO_2 in the JZB during winter

Temperature is an important thermodynamic parameter affecting seawater pCO_2. For example, the relationship between seawater temperature and pCO_2 proposed by Takahashi et al. (1993) shows that pCO_2 decreases by approximately 4.23% for every 1 °C decrease in water temperature. To assess the temperature effect on the pCO_2 distribution for each cruise, this study calculated npCO_2 by normalizing the surface pCO_2 at each station to the average seawater temperature in the corresponding cruise (see Section 2.3.3 Methodology). As shown in Figure 7a-g, in December (13th and 21st), early January (8th), mid-January (21st), and late January (26th), the pCO_2 in the upper end of the bay with lower temperatures increased by 20~65 μatm after normalization, while the pCO_2 in the mouth area of the bay with higher temperatures decreased by 15~30 μatm. This indicated that surface pCO_2 in the nearshore area was relatively low due to the cooling effect of land, whereas that in the mouth area was higher due to the frequent water exchange with the Yellow Sea where water temperature was relatively higher. In March (25th), the pCO_2 in the upper end of the bay with higher temperature decreased by ~12 μatm after normalization, while the pCO_2 in the mouth area with lower temperature increased by ~12 μatm, suggesting that land warming resulted in higher pCO_2 in the upper end area. All these results indicated the temperature effect on the spatial distribution of pCO_2 in certain periods of winter. However, combined with the distribution of *in situ* pCO_2 in each

cruise (Figure 4), in mid-January and late January, the *in situ* pCO_2 value in the northeastern area was lower than that in the mouth area by about ~80 μatm, which was larger than the contribution of pCO_2 (~50 μatm) caused by the difference in water temperature. In March, the *in situ* pCO_2 value in the northeastern was higher than that in the mouth area by about 50 μatm, which was also larger than the contribution of pCO_2 (~24 μatm) caused by the difference in water temperature. This indicated that the spatial distribution of pCO_2 was still largely affected by other factors. Even in some cruises, temperature may not be the main factor controlling pCO_2 distribution. For example, in December, *in situ* pCO_2 was the lowest in the mouth area with higher temperatures and the highest in the northeastern waters with lower temperatures. In late February, the difference between the highest and lowest seawater temperature was only 0.9 °C, but the difference in *in situ* pCO_2 was more than 160 μatm (Figures 4, 7).

The seawater surface temperature in the JZB experienced a pattern of first decrease and then increase from December to March. To assess the temperature effect on the pCO_2 variation between cruises, the NpCO_2 was calculated by normalizing the average seawater pCO_2 in each cruise to the average seawater temperature of all cruises (5.2 °C) (see Section 2.3.3 Methodology) (Figure 8). After normalization, the pCO_2 decreased by 33 μatm and 51 μatm in December and March, respectively, when the temperatures were relative higher; the pCO_2 increased by 20 μatm, 21 μatm, 47 μatm, and 12 μatm in early January, mid-January, late January and late February, respectively, when the temperatures were relative lower. The difference of pCO_2 between cruises decreased by 74% from December to early January and 52% from late February to March, but it only decreased by 8% from early January to late February. Moreover, the overall the temporal pattern of pCO_2 kept stable. The highest and lowest pCO_2 values still appeared in December and late February, respectively, and the difference between months was up to 130 μatm. It indicated that the temperature effect may play an important but not a dominant role in the whole intra-winter pCO_2 variation. Based on the method proposed by Takahashi et al. (2002) (see Section 2.3.3 Methodology), the relative contributions of temperature (T) and non-temperature effect (B) to pCO_2 variation throughout the winter were calculated. It is noteworthy that this method was originally designed for open oceanic systems and the non-temperature effect could be attributed almost entirely to the “net

biology effect". However, it had been widely used by other authors to assess the role of temperature versus biological factors in the control of pCO_2 dynamics in coastal areas (de la Paz et al., 2009; Ribas et al., 2011). The non-temperature term for coastal waters includes all the biogeochemical processes acting on CO_2. In this study, the T/B ratio was 0.81, indicating the main role of the non-temperature effect in intra-winter pCO_2 variation.

4.2 The non-conservative behaviour of DIC and TA and variation in the JZB during winter

In coastal waters, the non-temperature processes influencing pCO_2 mainly includes terrestrial input, biological processes (production/respiration), $CaCO_3$ processes (precipitation/dissolution), CO_2 sea-air exchange (evasion/invasion) and others. The occurrence of these processes often changes DIC and TA. Therefore, the analysis of DIC and TA non-conservative behaviour is helpful for identifying the main non-temperature factors for pCO_2 (Jiang et al., 2013; Li et al., 2017; Zhai et al., 2015). In some nearshore bays with no obvious runoff input, the ocean end-member can be used as a standard value to evaluate the effects of terrestrial input and biogeochemical processes, that is, the deviation of the measured DIC or TA from the ocean end-member. Thus, according to the approach of Jiang et al. (2013), the values for the addition or removal of DIC and TA in each cruise were obtained using the station data in the mouth area, which could represent the DIC and TA levels of the Yellow Sea, as the seawater end-member values (Li et al., 2017, Yang et al., 2018). In the specific calculation in late January, considering that the DO% in the mouth area was approximately 110% and a certain primary production existed (Figure 5e), this study chose the ocean end-member in mid-January, which was only 5 days apart. The calculation method is as follows:

$$\Delta DIC = DIC_i - \frac{S_i}{S_{ocean}} \times DIC_{ocean} \quad (8)$$

$$\Delta TA = TA_i - \frac{S_i}{S_{ocean}} \times TA_{ocean} \quad (9)$$

where ΔDIC and ΔTA represent the addition and removal of DIC and TA, respectively; and S_i (S_{ocean}), DIC_i (DIC_{ocean}), and TA_i (TA_{ocean}) are the salinity, DIC and TA of station i (the ocean end-member), respectively. This study used the average values of DIC and TA from the two stations, which had the highest salinity and were near the Yellow Sea, as the ocean end-member. The specific values are shown in Table 2.

As shown in Figure 9, the non-conservative behaviours of DIC and TA in the JZB presented three stages. First, ΔDIC and ΔTA maintained an addition status in the two cruises in December. The maximum addition values were observed in the northeastern area with low salinity and exceeded 200 μmol/kg, showing the effect of terrestrial DIC and TA input. The altered ratio of ΔDIC and ΔTA from terrestrial input was generally close to 1:1 (Cai et al., 2008), but the ΔDIC in the JZB was obviously larger than ΔTA in this period. Moreover, the difference between ΔDIC and ΔTA was the largest in the northeastern area (more than 90 μmol/kg), indicating that in addition to terrestrial input, other factors influenced DIC. Second, in the four cruises from early January to late February, ΔTA values also presented an addition status. However, there was a phenomenon that ΔDIC was less than ΔTA. In early January, this situation only occurred in the western area. In mid-January, this situation expanded to the entire bay. In late January and late February, the DIC showed partial or complete removal in different stations. The results indicated that DIC experienced an obvious consumption in this period. Finally, in March, both DIC and TA showed a removal status, and the removal of TA was greater than that of DIC. The maximum removals of TA and DIC were close to 30 μmol/kg and 20 μmol/kg, respectively. This suggested that the processes consuming DIC and TA existed in the meantime. Thus, the influences of non-temperature processes on pCO_2 were discussed in each period separately.

4.3 Aerobic respiration caused the bay to act as a CO_2 source in early winter

The biogeochemical processes that cause the non-conservative behaviour of DIC and TA could alter ΔDIC and ΔTA in fixed ratios. By comparing the ratio of ΔTA to ΔDIC at each station with the fixed ratios of the various processes that alter ΔTA and ΔDIC, the main processes causing the non-conservative behaviour of DIC and TA can be further clarified (Cai et al., 2004; Li et al., 2017; Liu et al., 2014). Throughout the winter in the low water period, the rivers flowing into the JZB had no natural runoff and the salinity in the northeastern area of the JZB was always the lowest. Therefore, the sewage discharge from the three wastewater treatment plants became the main source of terrestrial input, and the impact ratio of ΔDIC to ΔTA was approximately 1.03:1 (Li et al., 2017). For the production/respiration, the phytoplankton preferred NH_4-N as a nitrogen source in the JZB (Jiao, 1993). According to the Redfield equation with NH_4-N as the nitrogen source (Redfield, 1963),

404 the fixed ratio of ΔDIC to ΔTA altered by this process was 106:15. The fixed ratio of TA to DIC
405 altered by the $CaCO_3$ process was 2:1, and CO_2 evasion/invasion did not change TA while affected
406 DIC. Thus, the Figure 10 can be obtained.

407 The ΔTA/ΔDIC values in December were all located in the first quadrant, between the ratio
408 lines of direct treated sewage input and aerobic respiration (Figure 10 a, b). This indicated that the
409 DIC and TA additions were mainly caused by direct treated sewage input and aerobic respiration.
410 The total amount of daily treated sewage from the three wastewater treatment plants near the
411 northeastern area was 510,000 tons, and the DIC and TA concentrations of discharged sewage were
412 as high as 2554~5173 μmol/kg and 2326~4570 μmol/kg, respectively. Obviously, the direct input
413 of sewage was an important factor for the addition of DIC and TA in the northeastern area (Liu et
414 al., 2019; Yang et al., 2018). The impact of sewage on aquatic environment has been widely reported
415 in China (Yang et al., 2008; Yang et al., 2012). Meanwhile, the DO in the entire bay was unsaturated,
416 and the DO% was the lowest in the northeastern area with the highest pCO_2, which confirmed the
417 existence of an aerobic respiration process. Moreover, since aerobic respiration had little effect on
418 TA while increased DIC according the Redfield ratio, ΔDIC values were obviously larger than ΔTA
419 values in December. In addition, the influence of perennial urbanization and long water residence
420 time (~60 days, Liu et al., 2004) allowed the northeastern area of the bay to accumulate large
421 amounts of terrestrial materials (high DIC and TA input, organic matter, and others). Under the
422 strong vertical mixing in winter, the upwelling of bottom water would increase the DIC and TA in
423 surface seawater, and the organic matter carried from bottom would further promote aerobic
424 respiration and increase DIC.

425 After identifying that the main non-temperature processes which caused DIC and TA addition
426 in December were treated sewage input and aerobic respiration, the DIC/TA value was introduced
427 to explain their impacts on pCO_2. The DIC/TA value can directly indicate the relative abundance of
428 carbonate species (e.g., HCO_3^- and CO_3^-) in seawater. As such, for a specific temperature and
429 pressure, seawater surface pCO_2 is correlated with this ratio (Wang et al., 2013). The DIC/TA value
430 of treated sewage (1.03) was higher than that of the seawater (0.92~0.97) in the JZB. Therefore,
431 direct treated sewage input could increase the DIC/TA and pCO_2 of seawater in the northeastern

area. Meanwhile, aerobic respiration increased DIC by producing CO_2 directly and had a stronger increase effect on DIC/TA and pCO_2. The significant negative correlation between the npCO_2 (the temperature effect was removed) and DO% ($p < 0.05$) (Figure 11a) indicated that aerobic respiration had a dramatic effect on pCO_2 in the entire bay and it caused the bay to act as a CO_2 source in December. In the northeastern area with the lowest salinity, the degree of DO unsaturation was largest and the effects of treated sewage input were superimposed, so the pCO_2 was highest. As the sea area extended to the mouth area, the degree of DO unsaturation decreased gradually. The decline of aerobic respiration caused a gradual decrease in pCO_2 (Figure 11b). The dominant of aerobic respiration in December may be related to that the strengthened vertical mixing brought organic matters and the moderate temperature favoured the degradation activity of heterotrophic bacteria. The similar phenomenon was reported in the continental shelf off Georgia (USA) and the northern Yellow Sea (Jiang et al., 2010; Xu et al., 2016).

4.4 Primary production promoted the strength of CO_2 sink in winter

The distributions of ΔTA/ΔDIC in the four cruises from early January to late February are shown in Figure 10c-f. In the northeastern area in early January, ΔTA/ΔDIC values were similar to those in December, between the ratio lines of aerobic respiration and treated sewage input. This suggested that the DIC additions in this area were still mainly caused by these two processes. However, in the western area in early January and the entire bay in mid-January, all ΔTA/ΔDIC values were larger than 0.97 (the ratio of the treated sewage-altered ΔTA and ΔDIC), moving toward the ratio line of primary production. Considering the oversaturated DO in these periods and regions, the data indicated that primary production obviously consumed DIC, while the treated sewage input directly added DIC and TA. It is worth noting that the ΔTA/ΔDIC in these periods and regions were also close to the ratio lines of $CaCO_3$ dissolution and CO_2 evasion. This resulted from the coupled effects of direct treated sewage input and primary production because the possibility of $CaCO_3$ dissolution and CO_2 evasion were very low based on the high Ω_{arag}@situ (>1.80) and appearance of a CO_2 sink (Figures 4, 12). In late January and late February, the degree of DO oversaturation was higher and the ΔTA/ΔDIC values were closer to the ratio line of primary production, indicating the stronger consumption of DIC from primary production.

460 Obviously, the non-temperature processes affecting pCO_2 changed from aerobic respiration
461 in December to primary production during January and February, which caused an obvious decrease
462 in pCO_2 in the JZB (Figure 4). In the northeastern area of the JZB in early January, DO remained
463 unsaturated and aerobic respiration dominated and the region still acted as a CO_2 source. However,
464 in the western area in early January and the entire bay during mid-January, late January and late
465 February, DO was oversaturated and primary production dominated. The good correlations of
466 npCO_2 vs. DO% and Chl *a* vs. DO% (Figure 13) indicated that absorption of CO_2 by primary
467 production played an important role in the performance of the CO_2 sink in these periods and regions.
468 In the western area in early January, the DO was slightly oversaturated, and the primary production
469 began to dominate and turned the sea area from a CO_2 source in December into a sink. From mid-
470 January to late January, both DO supersaturation and Chl *a* concentration increased (Figure 5h), and
471 the correlation coefficients (r^2) of npCO_2 vs. DO% and DO% vs. Chl *a* also increased. The
472 enhancement of primary production continuously strengthened the CO_2 sink in the period (Figure
473 4h). In terms of the direct input of treated sewage, the increase in pCO_2 caused by this process was
474 persistent. However, the DO% was always the highest and the pCO_2 was always the lowest in the
475 northeastern area from mid-January to late February (Figures 4, 5), indicating that strong CO_2
476 consumption from primary production covered the increase in pCO_2 caused by direct input of treated
477 sewage.
478 The dominant of primary production in this period may be related to the relatively low
479 seawater temperature. The average seawater temperature had decreased obviously and was below
480 4 °C since early January and even below 2 °C in late January, which suppressed the activities of
481 aerobic respiration. Meanwhile, under stable hydrologic conditions and nutrient accumulation in
482 winter, the cold algae community, which had strong photosynthetic activity and was acclimatized to
483 low temperatures, often exhibited a vigorous growth in the JZB in January and February (Li and
484 Sun, 2014; Sun et al., 2011a; Wu et al., 2004). This is also the reasons for the vigorous growth of
485 phytoplankton in the nearshore areas of Hokkaido (Japan) and Blanca (Argentina) (Popovich et al.,
486 2008; Sakamoto et al., 2008). The weakening of feeding pressure caused by low temperatures may
487 be another reason. In Narragansett Bay, Oviatt et al. (2002) noted that the feeding effect from

zooplankton and filter feeders was inhibited and algal blooms usually occurred when the seawater temperature was below 3 °C. In Massachusetts Bay, Keller et al. (2011) found a good negative correlation between average Chl *a* concentration and seawater temperature during winters from 1995 to 1999 and they emphasized the control of zooplankton feeding on algal blooms.

4.5 The coupled effects of primary production and $CaCO_3$ precipitation on the pCO_2 in March

In March, all ΔTA/ΔDIC values fell in the third quadrant, basically between the ratio lines of primary production and $CaCO_3$ precipitation (Figure 10g). Combined with oversaturated DO and high Ω_{arag}@situ (2.28~2.53, Figure 12g), it could be inferred that the removal of DIC and TA was mainly caused by primary production and $CaCO_3$ precipitation. Compared to late February, both the DO oversaturation and the Chl *a* concentration decreased obviously in this period (Figure 5h). Thus, the weakening of primary production was an important factor causing the increase in pCO_2 in March. Meanwhile, npCO_2 showed no correlation with DO% (Figure 14a), indicating the reduced influence of primary production on the spatial distribution of pCO_2. In terms of $CaCO_3$ precipitation, this process consumed twice TA of DIC, and it further increased the pCO_2 levels in March. Considering that primary production consumed DIC but hardly affected TA, the degree of TA removal (ΔTA) could indicate the strength of $CaCO_3$ precipitation in the period. As shown in Figure 14b, npCO_2 was the highest in the northern area, where the TA removal was the largest (~-25 μmok/kg). As the sea area extended to the mouth area, TA removal and pCO_2 showed a decreasing trend. Obviously, the release of CO_2 from $CaCO_3$ precipitation had a certain influence on the spatial distribution of pCO_2 in March. Despite this, the losses of DIC and TA in March were all < 30 μmol/kg, indicating the small intensity of primary production and $CaCO_3$ precipitation. Moreover, due to the opposite effects on pCO_2 from the above two processes, the npCO_2 differences between the stations in this period were small, less than 30 μatm. In summary, in March, primary production and $CaCO_3$ precipitation together affected the concentration and spatial distribution of pCO_2 in the JZB.

The primary production may be constrained by the insufficient supply of nutrients in the bay in March. According to the observation between 2004 and 2008 (Sun et al., 2011b), the nutrient concentration in the JZB showed a gradual decrease from December to March and reached the minimum of < 0.2 mg/L in March. Meanwhile, the increase of feeding pressure caused by higher

seawater temperature also reduced the phytoplankton biomass (Zhang et al., 2005). The appearance of $CaCO_3$ precipitation in March may be related to the previously strong primary production in January and February. This is because large amounts of CO_2 consumption from primary production can increase the concentration of CO_3^{2-} and promote the rise of Ω_{arag}, which could increase the possibility of $CaCO_3$ precipitation (Kim et al., 2013; Xue et al., 2017). Meanwhile, the seawater temperature rose, and clams began to grow in spring (Zhang et al., 2005). The northern area of the JZB, where TA removal is the greatest, is an important breeding area for shellfish (*Ruditapes philippinarum*) in Qingdao, indicating that the appearance of $CaCO_3$ precipitation may be associated with human shellfish farming activities.

In summary, from aerobic respiration in December to primary production during January and February, and then to the weaken of primary production and the presence of $CaCO_3$ precipitation in March, the transition of non-temperature processes changed the JZB from a CO_2 source to sink and then to a weak sink throughout the winter. At the same time, the water temperature gradually decreased from December to late January and then increased until March, which suggested that the direction of temperature effect on pCO_2 was consistent with the non-temperature effect in most periods and temperature variation further expanded the pCO_2 variation range. Finally, according to the climatological mean wind speed in Qingdao from December to March (5.6 m/s, Yuan et al., 1996) and the average atmospheric CO_2 concentration (408 μatm) in the Tae-ahn Peninsula station from December 2015 to March 2016, the gas transfer velocity formula of Sweeney et al. (2007) was used to calculate the sea-air exchange fluxes of CO_2 (FCO_2). Overall, the JZB appeared as a sink of atmospheric CO_2 throughout the winter, with the average FCO_2 of -3.8 mmol m^{-2} d^{-1}. In December, the average FCO_2 of the two cruises was 3.0 mmol m^{-2} d^{-1}. Then the bay turned into an atmospheric CO_2 sink and the strength of sink continued to increase, from -6.4 mmol m^{-2} d^{-1} in early January to -15.5 mmol m^{-2} d^{-1} in late February. In March, the sink strength decreased obviously and the FCO_2 came to -1.1 mmol m^{-2} d^{-1}.

5. Conclusions

In the JZB from December to March, the mutual effect of non-temperature processes among aerobic respiration, primary production and $CaCO_3$ precipitation were the main intrinsic driving

forces for the pCO_2 variation. Meanwhile, the direction of temperature effect on pCO_2 was consistent with the non-temperature effect in most periods. In December, the higher seawater temperature and the dominance of respiration resulted in the bay acting as a CO_2 source. From early January to late January, with the decrease in pCO_2 caused by cooling, primary production of cold algae increased obviously and the Chl *a* concentration peaked in late February, with the consequence that the JZB became a larger CO_2 sink. In March, the seawater temperature rose, and the strength of CO_2 sink weakened obviously. In this period, with the decrease of primary production, the release of CO_2 from $CaCO_3$ precipitation appeared. The offsetting of these two processes resulted in a minor difference of the distribution of pCO_2. The strong biogeochemical process occurred widely in the mid-latitude coasts in winter, and its marked impact on seawater pCO_2 should not be ignored. To further improve our understanding of CO_2 sink/source change process and the influence factors in coastal waters, more field studies are still largely needed.

Acknowledgements

This work was supported by the National Natural Science Foundation of China (NSFC) (Grant No. 41376123), the National Natural Science Foundation of China - Shandong Joint Fund for Marine Science Research Centres (NSFC) (Grant No. U1406403) and the Science and Technology Foundation of Shanxi Agricultural University (Grant No. 2018YJ21). We thank Qianqian Jiang, Xiangyu Liu and Ping Han for the sampling and measuring work.

References

Bauer J E, et al, 2013. The changing carbon cycle of the coastal ocean. Nature, 504, 61-70.

Bianchi A A, et al, 2009. Annual balance and seasonal variability of sea-air CO_2 fluxes in the Patagonia Sea: Their relationship with fronts and chlorophyll distribution. Journal of Geophysical Research Oceans, 114(C03018).

Borges A V, 2011. Present day carbon dioxide fluxes in the coastal ocean and possible feedbacks under global change. Oceans and the Atmospheric Carbon Content, 47-77.

Bozec Y, et al, 2012. Seasonal dynamics of air-sea CO_2 fluxes in the inner and outer Loire estuary (NW Europe). Estuarine Coastal and Shelf Science, 100(1), 58-71.

Cai W J, et al, 2004. The biogeochemistry of inorganic carbon and nutrients in the Pearl River

estuary and the adjacent Northern South China Sea. Continental Shelf Research, 24(12), 1301-1319.

Cai W J, et al, 2008. A comparative overview of weathering intensity and HCO_3^- flux in the world's major rivers with emphasis on the Changjiang, Huanghe, Zhujiang (Pearl) and Mississippi rivers. Continental Shelf Research, 28(12), 1538-1549.

Cai W J, 2011. Estuarine and coastal ocean carbon paradox: CO_2 sinks or sites of terrestrial carbon incineration? Annual Review of Marine Science, 3(3), 123-145.

Chen C, et al, 1999. Influences of physical processes on the ecosystem in Jiaozhou Bay: a coupled physical and biological model experiment. Journal of Geophysical Research Oceans, 104, 29925-29949.

Chen C-T A, et al, 2013. Air-sea exchanges of CO_2 in the world's coastal seas. Biogeosciences, 10, 6509-6544.

Cohen J E, et al, 1997. Estimates of coastal populations, Science, 278, 1209-1213.

de la Paz M, et al, 2009. Surface fCO_2 variability in the Loire plume and adjacent shelf waters: High spatio-temporal resolution study using ships of opportunity. Marine Chemistry, 71(1), 55-64.

Dickson A G and Millero F J, 1987. A comparison of the equilibrium constants for the dissociation of carbonic acid in seawater media. Deep Sea Research Part A Oceanographic Research Papers, 34(10), 1733-1743.

Gao Z, et al, 2008. The land-sourced pollution in the Jiaozhou Bay. Chinese Journal of Oceanology and Limnology, 26(2), 229-232.

Gruber N, 2015. Ocean biogeochemistry: Carbon at the coastal interface. Nature, 517, 148-149.

Guillaud J F, et al, 2008. Seasonal variation of riverine nutrient inputs in the northern Bay of Biscay (France), and patterns of marine phytoplankton response. Journal of Marine Systems, 72(1-4), 309-319.

Heike L, et al, 2004. The pCO_2 variability in the midlatitude North Atlantic Ocean during a full annual cycle. Global Biogeochemical Cycles, 18, GB3023.

Jiang L Q, et al, 2010. Pelagic community respiration on the continental shelf off Georgia, USA. Biogeochemistry, 98(1), 101-113.

Jiang L Q et al, 2013. Influence of terrestrial inputs on continental shelf carbon dioxide. Biogeosciences, 10(2), 839-849.

Jiao N, 1993. Interactions between ammonium uptake and nitrate uptake by natural phytoplankton assemblages. Chinese Journal of Oceanology and Limnology, 11(2), 97-107.

Keller A A, et al, 2011. Phytoplankton production patterns in Massachusetts Bay and the absence of the 1998 winter-spring bloom. Marine Biology, 138(5), 1051-1062.

Kim D, et al, 2013. Biologically mediated seasonality of aragonite saturation states in Jinhae Bay, Korea. Journal of Coastal Research, 29(6), 1420-1426.

Laruelle G G, et al, 2014. Regionalized global budget of the CO_2 exchange at the air-water interface in continental shelf seas. Global Biogeochemical Cycles, 28, 1199-1214.

Lewis E and Wallace D W R, 1998. Program developed for CO_2 systems calculations. ORNL/CDIAC 105, Carbon Dioxide Information Analysis Center, Oak Ridge National Laboratory US Department of Energy, Oak Ridge, Tennessee.

Li J L and Sun X X, 2014. Photosynthetic characteristics of phytoplankton in winter in the Jiaozhou Bay. Oceanologia et Limnologia Sinica, 3(45), 468-479. (in Chinese).

Li N, et al, 2006. Natural environment and geological evolution of Jiaozhou Bay. Ocean Press, Beijing (in Chinese).

Li X, et al, 2007. Role of the Jiaozhon Bay as a source/sink of CO_2 over a seasonal cycle. Scientia Marina, 71(3), 441-450.

Li Y, et al, 2017. Controlling mechanisms of surface partial pressure of CO_2 in Jiaozhou Bay during summer and the influence of heavy rain. Journal of Marine Systems, 173, 49-59.

Liu Z, et al, 2004. Simulation of water exchange in Jiaozhou Bay by average residence time approach. Estuarine Coastal and Shelf Science, 61(1), 25-35

Liu Z, et al, 2014. Removal of dissolved inorganic carbon in the Yellow River Estuary. Limnology and Oceanography, 59(2), 413-426.

Liu X Y, et al, 2019. Variations in dissolved inorganic carbon species in effluents from large-scale municipal wastewater treatment plants (Qingdao, China) and their potential impacts on coastal acidification. Environmental Science and Pollution Research, 26, 15019-15027.

628 Ljubimir S, et al, 2017. Interannual (2009-2013) variability of winter-spring phytoplankton in South
629 Adriatic Sea: effects of deep convection and lateral advection. Continental Shelf Research, 143,
630 311-321.
631 Mehrbach C, et al, 1973. Measurement of the apparent dissociation constants of carbonic acid in
632 seawater at atmospheric pressure. Limnology and Oceanography, 18(18), 897-907.
633 Millero F J, 1979. The thermodynamics of the carbonate system in seawater. Geochimica Et
634 Cosmochimica Acta, 43(10), 1651-1661.
635 Miyazawa Y, et al, 2017. Assimilation of high-resolution sea surface temperature data into an
636 operational nowcast/forecast system around Japan using a multi-scale three-dimensional
637 variational scheme. Ocean Dynamics, 67(6), 713-728.
638 Mucci A, 1983. The solubility of calcite and aragonite in seawater at various salinities, temperatures,
639 and one atmosphere total pressure. American Journal of Science, 283(7), 14-27.
640 Nakaoka S I, et al, 2006. Temporal and spatial variations of oceanic pCO_2 and air–sea CO_2 flux in
641 the Greenland Sea and the Barents Sea. Tellus 58B, 148-161.
642 Oviatt C, et al, 2002. Annual primary production in Narragansett Bay with no bay-wide winter-
643 spring phytoplankton bloom. Estuarine Coastal and Shelf Science, 54(6), 1013-1026.
644 Popovich C A, et al, 2008. Dissolved nutrient availability during winter diatom bloom in a turbid
645 and shallow estuary (Bahía Blanca, Argentina). Journal of Coastal Research, 24(1), 95-102.
646 Redfield A C, 1963. The influence of organisms on the composition of seawater. In: Hill, M.N. (Ed.),
647 The Sea. vol. 2. Interscience, pp. 26–77.
648 Ribas-Ribas M, et al, 2011. Air–sea CO_2 fluxes in the north-eastern shelf of the Gulf of Cádiz
649 (southwest Iberian Peninsula). Marine Chemistry, 123(1-4), 56-66.
650 Sakamoto A, et al, 2008. Time series of carbonate system variables off Otaru coast in Hokkaido,
651 Japan. Estuarine Coastal and Shelf Science, 79(3), 377-386.
652 Sun X, et al, 2011a. Long- term changes of chlorophyll a concentration and primary productivity in
653 the Jiaozhou Bay. Oceanologia et Limnologia Sinica, 42(5), 654-661. (in Chinese).
654 Sun X, et al, 2011b. Long- term changes in nutrient concentration and structure in the Jiaozhou Bay.
655 Oceanologia et Limnologia Sinica, 42(5), 662-669. (in Chinese).

Sweeney C, et al, 2007. Constraining global air-sea gas exchange for CO_2 with recent bomb ^{14}C measurements. Global Biogeochemical Cycles, 21, GB2015.

Takahashi T, et al, 1993. Seasonal variation of CO_2 and nutrients in the high-latitude surface oceans: a comparative study. Global Biogeochemical Cycles, 7(4), 843-878.

Takahashi T, et al, 2002. Global sea–air CO_2 flux based on climatological surface ocean pCO_2 and seasonal biological and temperature effects. Deep Sea Research Part II: Topical Studies in Oceanography, 49(9-10), 1601-1622.

Tin H C, et al, 2016. Satellite-derived estimates of primary production during the Sargasso Sea winter/spring bloom: Integration of in-situ time-series data and ocean color remote sensing observations. Regional Studies in Marine Science, 3, 131-143.

Thomas H, et al, 2005. Controls of the surface water partial pressure of CO_2 in the North Sea. Biogeosciences, 2(4), 323-334.

Wang B and Wang Z, 2011. Long-term variations in chlorophyll a and primary productivity in Jiaozhou Bay, China. Journal of Marine Biology, 1-6.

Wang Y J, et al, 2015. Temporal and spatial variations of chlorophyll a and environmental factors in Jiaozhou Bay in 2010–2011. Acta Oceanologica Sinica, 37 (4), 103–116 (in Chinese).

Wang Z A, et al, 2013. The marine inorganic carbon system along the Gulf of Mexico and Atlantic coasts of the United States: Insights from a transregional coastal carbon study. Limnology and Oceanography, 58(1), 325-342.

Wanninkhof R, et al, 2013. Global ocean carbon uptake: magnitude, variability and trends. Biogeosciences, 10(3), 1983-2000.

Wesslander K, et al, 2010. Inter-annual variation of the air-sea CO_2 balance in the southern Baltic Sea and the Kattegat. Continental Shelf Research, 30, 1511-1521.

Wu Y, et al, 2004. Quantitative study in long-term variation of phytoplankton in Jiaozhou Bay. Oceanologia et Limnologia Sinica, 35 (6), 518-523 (in Chinese).

Xu X, et al, 2016. Monthly CO_2 at A4HDYD station in a productive shallow marginal sea (Yellow Sea) with a seasonal thermocline: Controlling processes. Journal of Marine Systems, 159, 89-99.

Xue L, et al, 2012. Surface partial pressure of CO_2, and air–sea exchange in the northern Yellow Sea. Journal of Marine Systems, 105-108(12), 194-206.

Xue L, et al, 2017. Sea surface aragonite saturation state variations and control mechanisms at the Gray's Reef time-series site off Georgia, USA (2006–2007). Marine Chemistry, 195, 27-40.

Yang H, et al., 2008. Carbon source/sink function of a subtropical, eutrophic lake determined from an overall mass balance and a gas exchange and carbon burial balance. Environmental Pollution, 151, 559-568.

Yang H, et al., 2012. Pollution in the Yangtze. Science, 337, 410.

Yang W, et al, 2007. Preliminary study on effects of scallop cultivation on water quality in Jiaozhou Bay. Transactions of Oceanology and Limnology, (2), 86-93 (in Chinese).

Yang X, et al, 2018. Treated wastewater changes the export of dissolved inorganic carbon and its isotopic composition and leads to acidification in coastal oceans. Environmental Science and Technology, 52, 5590-5599.

Zang H, et al, 2018. The contribution of low temperature and biological activities to the CO_2 sink in Jiaozhou Bay during winter. Journal of Marine Systems, 186, 37-46.

Zhang J H, et al, 2005. Clearance rate, ingestion rate and absorption efficiency of cultivated clam *ruditapes philippinarum* in Jiaozhou Bay, China. Oceanologia et Limnologia Sinica, 36 (6), 548-555. (in Chinese)

Zhang L, et al, 2012. Distribution and seasonal variation in the partial pressure of CO_2 during autumn and winter in Jiaozhou Bay, a region of high urbanization. Marine Pollution Bulletin, 64(1), 56-65.

Zhai W, et al, 2015. Occurrence of aragonite corrosive water in the North Yellow Sea, near the Yalu River estuary, during a summer flood. Estuarine Coastal and Shelf Science, 166, 199-208.

Zhao Q, et al, 2004. Winter and summer chlorophyll a and nutrient distribution and characteristics in the Bohai Sea. Marine Sciences, 28 (4), 34–39 (in Chinese).

Figure captions

Figure 1. Study area and survey stations. Solid black circles represent the sampling stations and white stars represent wastewater treatment plants. The gray scale shows water depth.

Figure 2. Variations in seawater surface salinity and temperature during the seven cruises in the JZB. The solid black and open blue squares represent the average seawater surface temperature and salinity. The upper and lower error bars represent the maximum and minimum of seawater surface temperature (salinity) in the cruise. The thick gray line represents the daily average seawater temperature in the JZB from December to April during the period of 2008-2016. The daily seawater temperature data were from FRA-JCOPE2 reanalysis data in Japan (http://www.jamstec.go.jp/jcope/htdocs/e/home.html) and were calculated using the JCOPE2 model according to satellite data (for more method details, please refer to Miyazawa et al. (2017)).

Figure 3. Spatial distributions of seawater surface salinity and temperature during the seven cruises in the JZB. The isoline represents salinity and the color scale shows temperature.

Figure 4. Spatial distributions of seawater surface pCO_2 during the seven cruises in the JZB (a-g). Mean pCO_2 during the seven cruises and the upper and lower error bars represent the maximum and minimum of pCO_2 in each cruise (h).

Figure 5. Spatial distributions of seawater surface DO% and Chl *a* during the seven cruises in the JZB (a-g). The isoline represents Chl *a* and the color scale shows DO%. The mean DO% and Chl *a* during the seven cruises and the upper and lower error bars represent the maximum and minimum of DO% (Chl *a*) in each cruise (h).

Figure 6. Spatial distributions of seawater surface DIC and TA during the seven cruises in the JZB. The isoline represents DIC and the color scale shows TA.

738 **Figure 7.** Spatial distributions of ΔpCO_2 during the seven cruises in the JZB. ΔpCO_2 represents the
739 difference between npCO_2 and *in situ* pCO_2. The npCO_2 represents the *in situ* pCO_2 normalized to
740 the average seawater temperature for each cruise.
741
742 **Figure 8.** Variations in pCO_2 (solid circle) and NpCO_2 (open circle) during the seven cruises.
743 NpCO_2 represents the average pCO_2 for each cruise normalized to the average seawater temperature
744 of all seven cruises.
745
746 **Figure 9.** Scatterplot of ΔDIC (red triangle) and ΔTA (black circle) with salinity in the JZB during
747 the seven cruises. ΔTA and ΔDIC are deviations calculated using Equations. 8 and 9.
748
749 **Figure 10.** Scatterplot of ΔTA vs. ΔDIC in the JZB during the seven cruises. The four lines represent
750 the theoretical ratio lines altered the ΔTA and ΔDIC by the direct treated sewage input, $CaCO_3$
751 precipitation/dissolution, biological process (primary production or respiration) and CO_2
752 evasion/invasion, respectively. The stations in northeastern area and western area were located in
753 the solid and dotted line circles in c, respectively. Color scale shows DO%.
754
755 **Figure 11.** Scatterplot of npCO_2 vs. DO% (a) and DO% vs. salinity (b) on 13 December (solid
756 circles, y_1) and 21 December (open squares, y_2).
757
758 **Figure 12.** Spatial distributions of seawater surface Ω_{arag}@situ during the seven cruises in the JZB.
759
760 **Figure 13.** Scatterplot of npCO_2 vs. DO% (a) and DO% vs. Chl *a* (b) in western area in early January
761 (solid triangles, y_1) and the entire bay in mid-January (open circles, y_2), late January (solid squares,
762 y_3) and late February (stars, y_4).
763
764 **Figure 14.** Scatterplot of npCO_2 vs. DO% (a) and npCO_2 vs. ΔTA (b). The open circles represent
765 the stations in northern area of the JZB.

766

767 **Table. 1.** Summary of the sampling cruises. In late February, we only referenced the data covering

768 our research stations.

769

770 **Table. 2.** The values of salinity, DIC and TA of ocean end-member in each cruise during winter in

771 the JZB.

772 **Figures**

773 **Figure 1.**

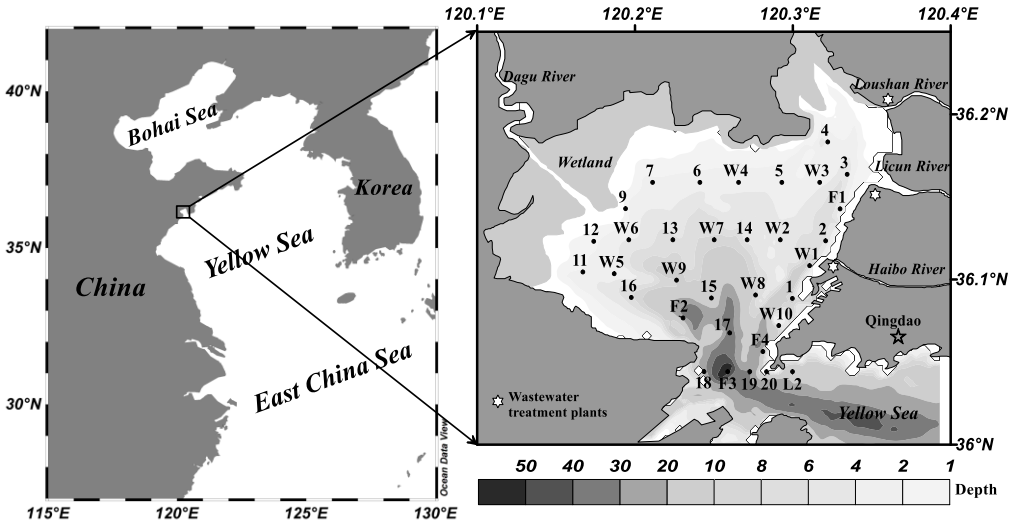

774

775 **Figure 2.**

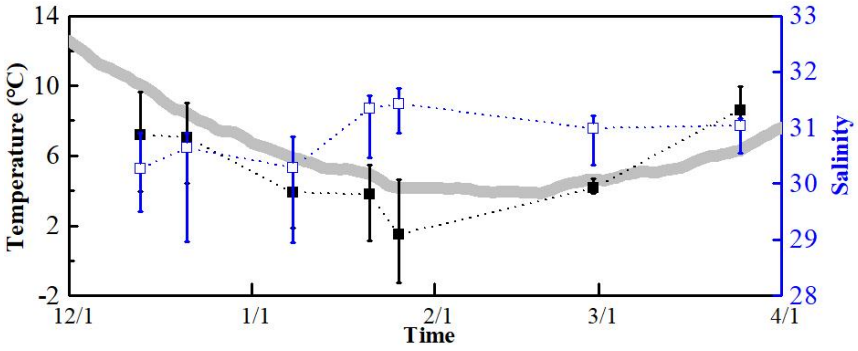

776

777

Figure 3.

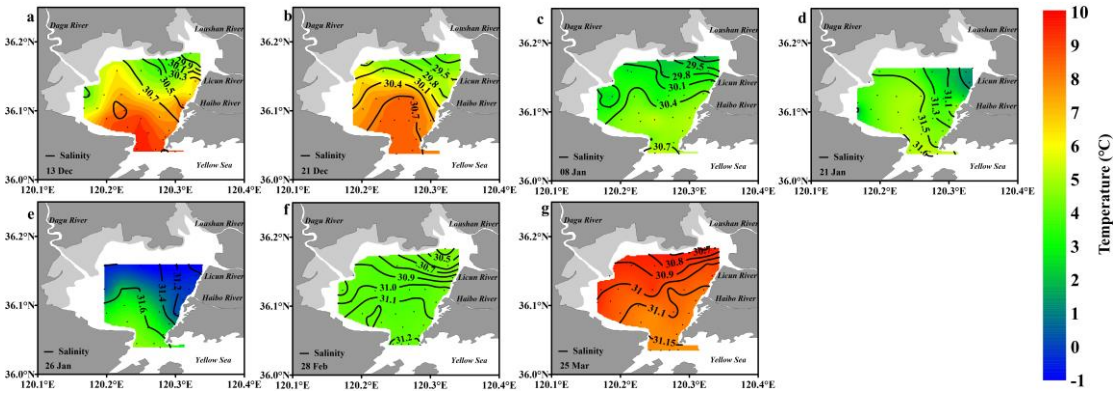
a
b
c
d
e
f
g
Daqu River
Laoshan River
Licun River
Haibo River
Yellow Sea
Salinity
13 Dec
21 Dec
08 Jan
21 Jan
26 Jan
28 Feb
25 Mar
36.2°N
36.1°N
36.0°N
120.1°E
120.2°E
120.3°E
120.4°E
Temperature (°C)
10
9
8
7
6
5
4
3
2
1
0
-1

781 **Figure 4.**

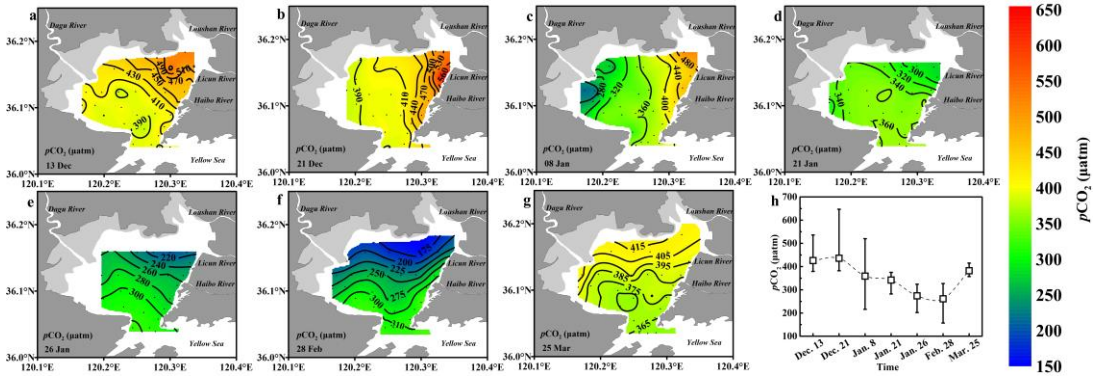

782

783

Figure 5.

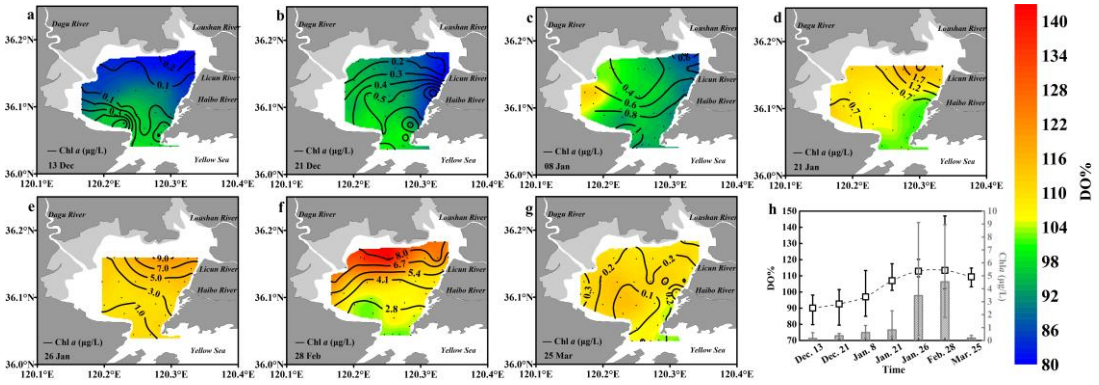
a
b
c
d
e
f
g
h
Daqu River
Laoshan River
Licun River
Haibo River
Yellow Sea
— Chl a (μg/L)
13 Dec
21 Dec
08 Jan
21 Jan
26 Jan
28 Feb
25 Mar
36.2°N
36.1°N
36.0°N
120.1°E
120.2°E
120.3°E
120.4°E
DO%
Chl a (μg/L)
Time
Dec. 13
Dec. 21
Jan. 8
Jan. 21
Jan. 26
Feb. 28
Mar. 25
140
134
128
122
116
110
104
98
92
86
80

Figure 6.

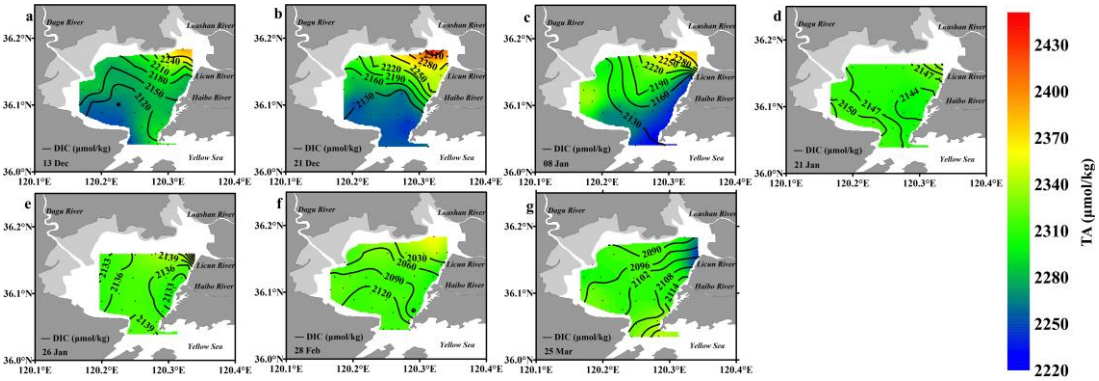
a
b
c
d
e
f
g
Dagu River
Laoshan River
Licun River
Haibo River
Yellow Sea
— DIC (μmol/kg)
13 Dec
21 Dec
08 Jan
21 Jan
26 Jan
28 Feb
25 Mar
120.1°E
120.2°E
120.3°E
120.4°E
36.2°N
36.1°N
36.0°N
2430
2400
2370
2340
2310
2280
2250
2220
TA (μmol/kg)

Figure 7.

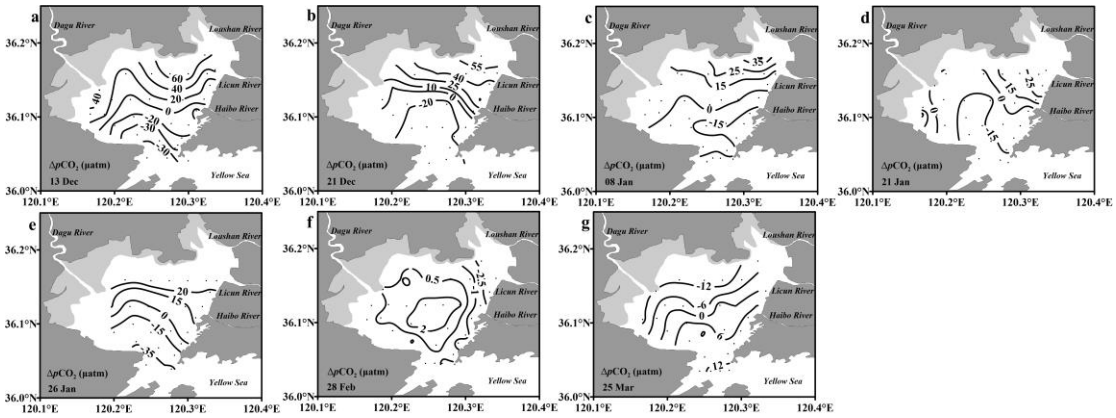
a
b
c
d
e
f
g
Daqu River
Laoshan River
Licun River
Haibo River
Yellow Sea
ΔpCO2 (μatm)
13 Dec
21 Dec
08 Jan
21 Jan
26 Jan
28 Feb
25 Mar
36.2°N
36.1°N
36.0°N
120.1°E
120.2°E
120.3°E
120.4°E

793 **Figure 8.**

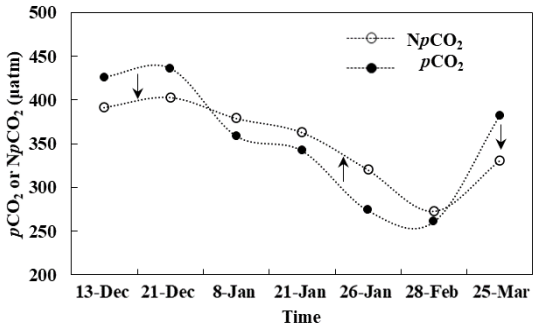

794

795

Figure 9.

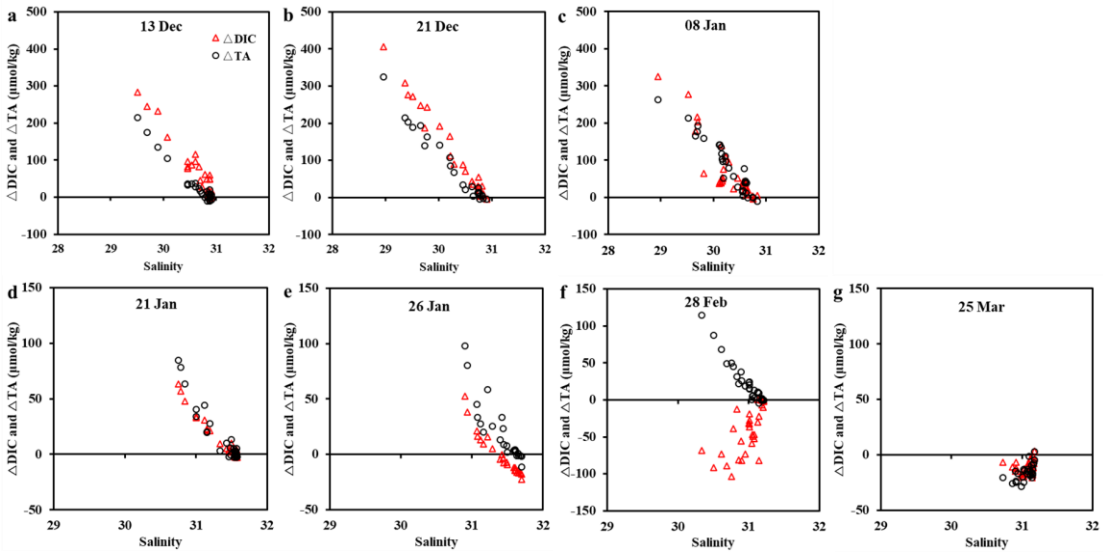
a
13 Dec
△DIC
△TA
b
21 Dec
c
08 Jan
d
21 Jan
e
26 Jan
f
28 Feb
g
25 Mar
△DIC and △TA (μmol/kg)
Salinity

Figure 10.

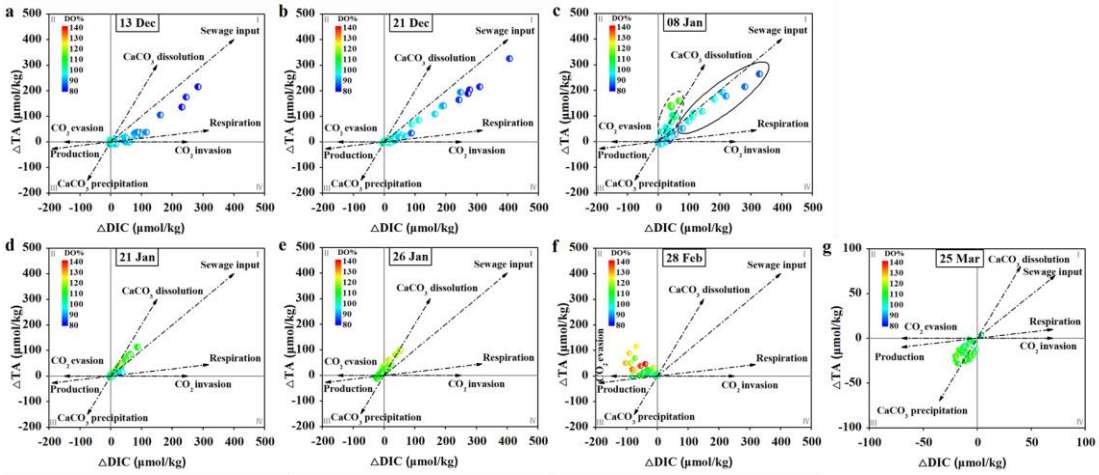
a
13 Dec
b
21 Dec
c
08 Jan
d
21 Jan
e
26 Jan
f
28 Feb
g
25 Mar
DO%
Sewage input
CaCO3 dissolution
CO2 evasion
Respiration
Production
CO2 invasion
CaCO3 precipitation
ΔTA (μmol/kg)
ΔDIC (μmol/kg)

802 **Figure 11.**

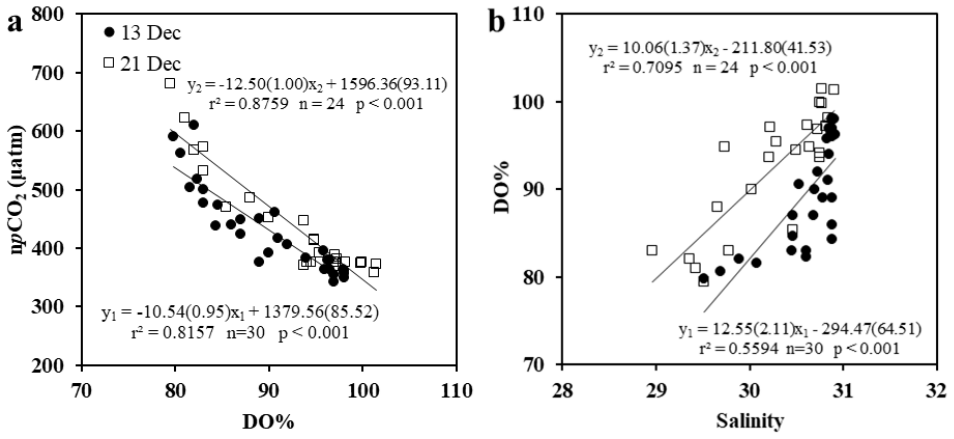

803

804

Figure 12.

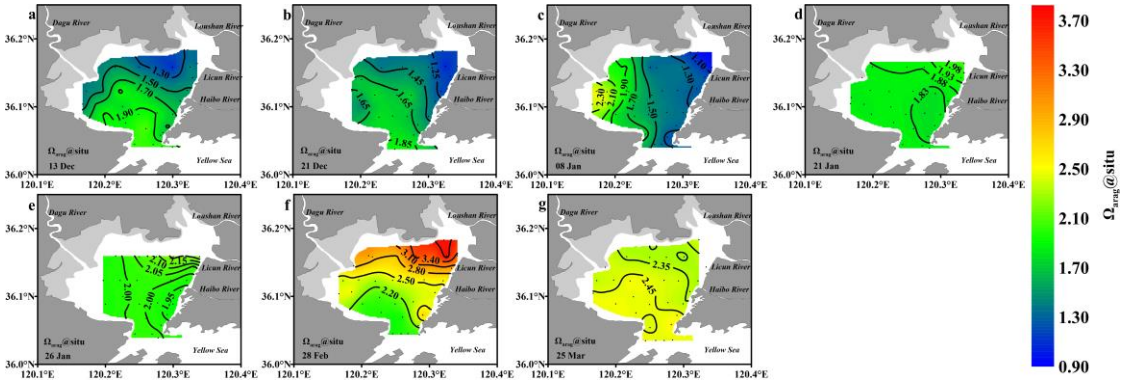
a
b
c
d
e
f
g
Daqu River
Laoshan River
Licun River
Haibo River
Yellow Sea
13 Dec
21 Dec
08 Jan
21 Jan
26 Jan
28 Feb
25 Mar
36.2°N
36.1°N
36.0°N
120.1°E
120.2°E
120.3°E
120.4°E
3.70
3.30
2.90
2.50
2.10
1.70
1.30
0.90
Ωarag@situ

808 **Figure 13.**

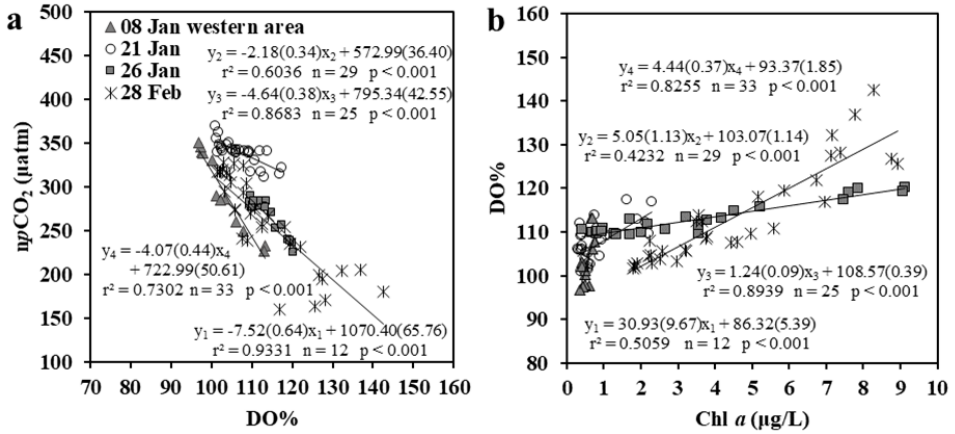

809

810

811 **Figure 14.**

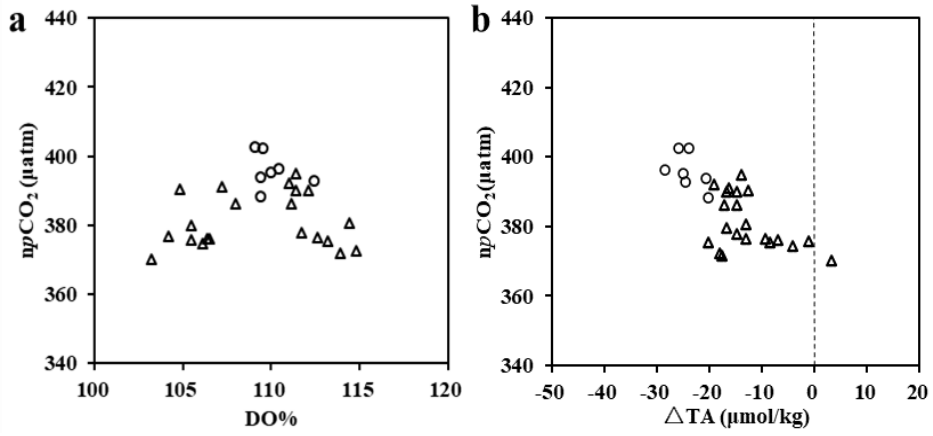

812

813

814 **Table. 1.**

Cruise	Surveying time	Number of stations	Reference/data source
December	13 Dec. 2014	30	This study
	21 Dec. 2011	24	This study
Early January	08 Jan. 2012	33	This study
Mid-January	21 Jan. 2016	29	Zang et al. (2018)
Late January	26 Jan. 2016	25	Zang et al. (2018)
Late February	28 Feb. 2008	33	Zhang et al. (2012)
March	25 Mar. 2014	30	This study

815

816 **Table. 2.**

Cruise	S_{ocean}	DIC_{ocean}	TA_{ocean}
13 Dec	30.88±0.00	2102±2	2277±1
21 Dec	30.84±0.07	2088±1	2255±1
08 Jan	30.75±0.00	2117±4	2240±0
21, 26 Jan	31.55±0.00	2147±1	2310±0
28 Feb	31.21±0.00	2140±2	2314±1
25 Mar	31.17±0.00	2122±0	2344±0

817